J. Condensed Matter Nucl. Sci. 25 (2017) 1–25

Research Article

Observation of Excess Heat by Activated Metal and Deuterium Gas

Tadahiko Mizuno*

Hydrogen Engineering Application and Development Company, Kita 12, Nishi 4, Kita-ku, Sapporo 001-0012, Japan

Abstract

Reports of heat-generating cold fusion reactions in the nickel–hydrogen system have been increasing. The reactions mainly involve nickel with other additive elements. The authors of these reports emphasized the importance of an extremely clean system in the electrolytic tests in which excess heat was generated. Therefore, we attempted to detect excess heat after reducing impurities to a minimum by cleaning the electrode carefully and then fabricating nanoparticles in situ in our test system, without ever exposing them to air. As a result, energy far exceeding input was continuously obtained. In the best results obtained thus far, the output thermal energy is double the input electrical energy, amounting to several hundred watts. The generated thermal energy follows an exponential temperature function. When the reactor temperature is 300°C, the generated energy is 1 kW. An increase of the temperature is expected to greatly increase the output energy. We have recently improved the preparation of the electrode material. This enhanced reproducibility and increased excess heat. The new methods are described in the Appendix.
 ISSN 2227-3123

Keywords: Deuterium gas, Heat generation, Ni metal, Surface activation

1. Introduction

We have aimed to reproduce a long-standing curious phenomenon that occurs in metal–hydrogen systems [1–5]. At first, the reaction was assumed to be a normal nuclear fusion reaction, so confirmation experiments involving neutron detection during the electrolysis of heavy water were conducted [6]. Focus then shifted to analysis of the elements isotopically changed during electrolysis. The generation of heat in the process, which had rarely been observed, became a recurring phenomenon [7–10]. The heat-generating reaction of a nickel–hydrogen system, in particular, has been reported [11–13]. This system, when compared to the initial Pd–D_2 system has been regarded as a null calibration test. The generation of excess heat in reactions involving nickel was observed with additive elements in these reports. However, the authors noted the importance of a very clean system in early electrolysis tests where excess heat was observed. Therefore, in the present work, we eliminated impurities in an attempt to detect excess heat. Specifically, we developed a very simple heat estimation analysis, based on flowing air calorimetry, to confirm excess heat induced by the reaction between hydrogen and a metal. The factors considered are only the amount of air and the temperature difference between the air flowing into and out of the calorimeter. These factors contribute the most to heat analysis

*E-mail: head-mizuno@lake.ocn.ne.jp

 ISSN 2227-3123

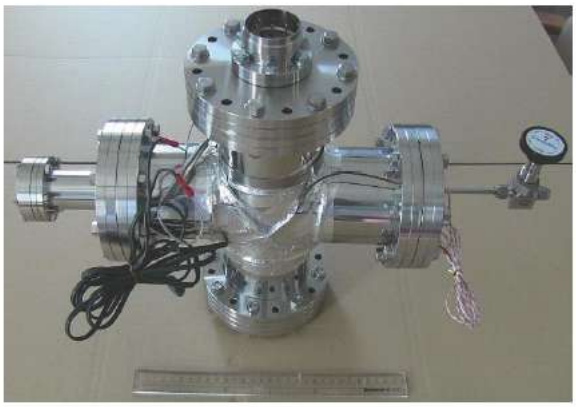

Figure 1. Photo of the reactor body. The upper part is the electrode inlet part, on the left is the viewing window, and the gas valve is seen on the right. A heating wire is wrapped around the reactor body center part. The connecting wire and platinum temperature sensor can be seen.

and can easily be used estimate the excess heat. In this paper we describe the excess heat in a simple metal–hydrogen system.

2. Experiment

2.1. Reactor body

The reactor body is a cruciform cylindrical shape as shown in Fig. 1. All parts are connected with metal seal flanges. The upper part of the reactor comprises the heater power inlet, the high-voltage discharge electrode, and a thermocouple. Several platinum temperature measuring elements (Okazaki; Pt AA class $\pm(0.1+0.0017|t|) - 196 \sim 450$) were installed in the reactor. As shown in Fig. 1, there is a Kovar glass window on the left-hand side of the reactor, and a pressure gauge; and a mass spectrometer valve and the gas inlet valve is on the right-hand side. A vacuum evacuation system and a quadrupole gas analysis system are connected to the body.

The reactor is made of SUS 316. Its volume is 2740 cm^3 and its weight is 20.3 kg.

2.2. Reaction material

The inner wall surface of the reactor was covered with two pieces of nickel mesh (99.9%, Ni 200 alloy, 180 mesh, Inada Wire Mesh Co. Ltd.) the wire diameter is 0.055 mm, the total wire length is 896 m, and the surface area is 0.31 m^2. Each mesh was 300 $\times$ 300 mm^2 and composed of 0.15-mm-diameter wire; the opening size was 180 mesh, and the total weight was 23 g. Figure 2 is a photo of the Ni mesh. The Ni mesh is first degreased with detergent. It is then installed against the wall inside the reactor.

The two meshes were installed in the center of the reactor inner surface. The nickel meshes were unrolled and pressed with a nickel plate (thickness 0.5 mm, width 5 mm, length 500 mm) against the reactor inner surface to ensure contact with the inner wall of the reactor, which is necessary to maintain thermal conduction. Figure 3 shows a view of the mesh and the reactor. The mesh is in tight contact with the inner wall of the reactor. This photo shows the reactor, flange, and mounting hole. A copper gasket can be seen on the flange surface. The Ni mesh in the reactor and body is prepared by cleaning with high temperature pure water for 1 h, and washed with alcohol and acetone.

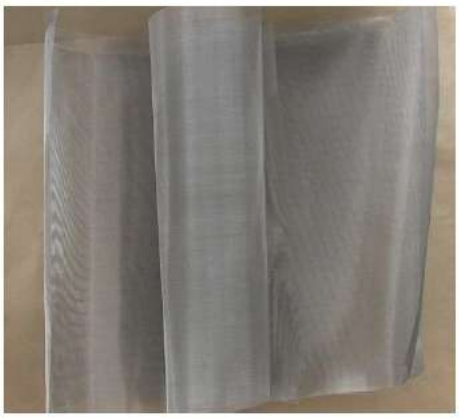

Figure 2. Nickel mesh as reactant, 30 cm^2, 200 mesh. This photo shows the two meshes overlapped.

2.3. Inner arrangement of reactor

Figure 4 shows the upper parts of the reactor and cross section of the reactor. Two high-voltage electrodes and one electric power inlet for a small ceramic heater and an inlet for a thermocouple were installed in the reactor as shown in the left-hand side of Fig. 4. In Fig. 4, the electrode on the left-hand inside the reactor, which was for discharge, was a 50-mm-long, 3-mm-diameter palladium tube wound with 200 mm of 1-mm-diameter palladium wire (weight 2.82 g). This electrode was insulated from the reactor body. The gas temperature around the electrode was measured with a stainless-steel-coated K-type thermocouple with a diameter of 1.6 mm and a length of 300 mm. The thermocouple was insulated in a 3-mm-diameter, 100-mm-long alumina tube to prevent it from being affected by the plasma discharge. The other input terminal is for high voltage power supply to the Pd wire wound around the heater. The tip of this terminal leads to the Pd thin wire wound around the heater. A high voltage current is supplied from the terminal to the

Figure 3. View of Ni mesh in the reactor.

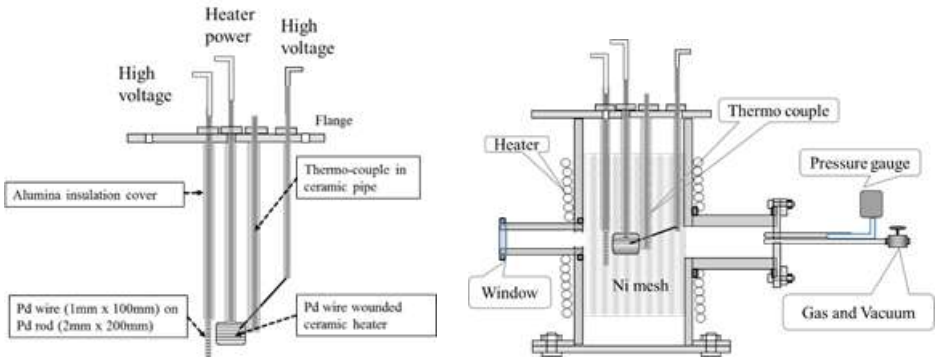

Figure 4. Schematic representation of electrode and cross section of reactor.

Pd fine wire. An aluminum ceramic heater with a maximum temperature of 1000°C was positioned in the reactor's center. The heater was 30 × 30 mm^2, with a thickness of 2 mm. A K-type thermocouple was positioned near the heater. A palladium wire with a diameter of 0.3 mm length 200 mm, was wound around the heater.

The cross section in Fig. 4 (right-hand side) shows the electrodes inside the reactor, and the internal ceramic heater. It also shows the condition of the nickel mesh. The figure is a conceptual diagram, but it depicts the internal state accurately. In this figure, a heater, valves, and so on are drawn around the reactor body. This is explained below.

Figure 5 shows a photo of the tip of the ceramic heater, Pd fine wire and Pd discharge electrode in the reaction

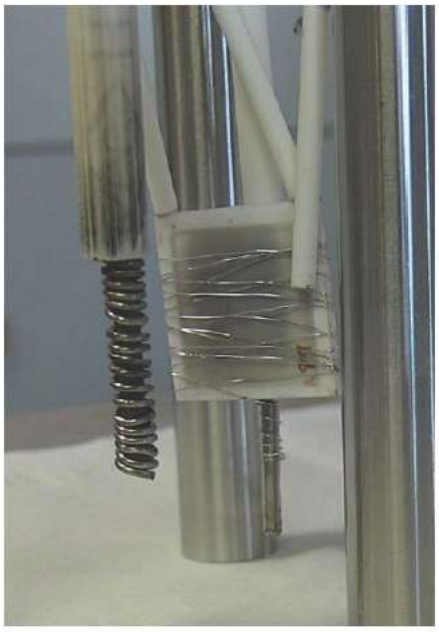

Figure 5. View of the electrode and heater in the reactor.

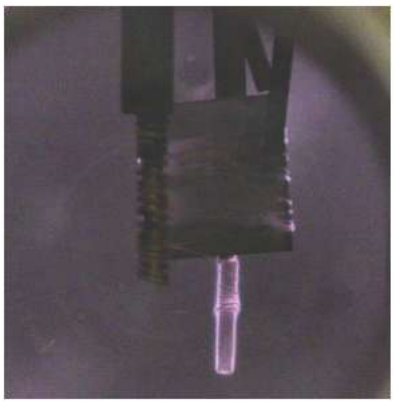

Figure 6. Photo of plasma state when discharging by applying a high voltage to the Pd thin wire on the ceramic heater.

reactor. In the photograph, two thick metal columns are provisional supports are needed while working to attach the electrodes. They are removed when the structure is placed in the reactor body. Pd fine wire is coarse wrapped around the ceramic heater. This heater is heated to evaporate the Pd metal. There is a Pd rod to supply high voltage current under the heater, and a thin wire is wound around it. The ceramic tube on the upper right of the ceramic heater is in contact with the heater. A thermocouple is contained inside this ceramic tube. Two ceramic tubes at the top of the heater are for the power supply to the ceramic heater, with a small copper wire.

2.4. Reactor heater

A 2-m-long heater of stainless sheath was wrapped around the reactor body. Its purpose was to heat the nickel mesh in the reactor. The heater capacity is 100 V, 600 W, with a maximum temperature of 500°C. Six platinum temperature measuring elements were attached to various parts of the reactor. The heater was covered by thick aluminum tape around the heater several times to make the temperature distribution of the reactor uniform, as shown in Fig. 1.

2.5. Preparation of reacting material

The Ni mesh around the inner surface of the reactor is discharged by high voltage of DC current between the wire around the heater electrode and another Pd wire electrode. The reaction gas is 99.9% pure deuterium (Nippon Oxygen).

The electrode preparation treatment procedure is as follows:

(1) The gas in the reactor is evacuated to several Pa of pressure.
(2) D_2 gas is supplied to the reactor at several hundred Pa.
(3) Electric power to the heater around the reactor is supplied at 50 W for 10 h, and the temperature of the reactor reaches around 50°C.
(4) The gas in the reactor is evacuated to $\sim$40 Pa.
(5) High voltage is supplied to the wire around the ceramic heater. Plasma is formed. At this stage, if the plasma is difficult to generate you can increase input voltage, but it is better to keep the D_2 gas pressure below 50 Pa. The current becomes stable at $\sim$40 mA. The state of the glow discharge at this time is shown in Fig. 6. Gas is emitted from the heater wound around the ceramic, and the light from the gas can be seen. The part covered

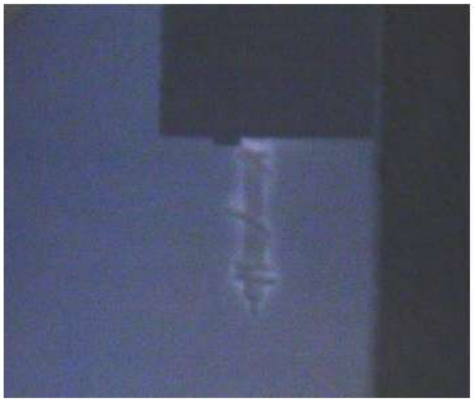

Figure 7. Photo of plasma state in which a high voltage is applied to the Pd thin wire on the ceramic heater.

with the lower pink and violet color plasma is Pd winding which supplies high voltage to the Pd thin wire. It is still covered with same color of plasma and gas which is released from the inside of the reactor.

This discharge is continued for several hours. With this process, the pressure in the reactor increases over time. This is because gases absorbed in the sample and the reactor body are released. If this gas release stops and the pressure does not change, the discharge can be stopped.

Additional procedures are performed:

(6) When the impurity gas release stops, gas inside the reactor is again evacuated while heating the reactor body.
(7) New D_2 gas is then supplied at 50 Pa, with 100 W of input power to the reactor heater. When the temperature has stabilized, that is, when it reaches approximately 100°C, the high voltage current is again supplied to the Pd fine wire around the ceramic heater. Discharge starts at around 500 V. If the glow discharge does not appear, voltage is increased until it appears. The discharge is continued for several hours. Then the pressure in the reactor is increased again.
(8) The pressure inside the reactor finishes increasing, and when stabilized, the reactor is again evacuated.

During Steps 7 and 8 the reactor temperature is gradually raised up to 350°C. When residual gas stops coming out from the reactor and the amount of D_2 gas component is large, a light blue discharge appears, as shown in Fig. 7. This is observed at a pressure of less than 5 Pa. When the impurity gas disappears, while keeping the reactor temperature high, the D_2 gas is finally supplied at 500 Pa and the heating of the reactor is stopped. The operator then waits until the temperature drops to room temperature.

When the temperature drops to room temperature, gas is evacuated from the furnace down to 50 Pa or less. Thereafter, a current with a high voltage of 500 V is supplied to the electrode on which the Pd wire is wound around the Pd rod. If discharge is difficult to start, the gas pressure is lowered to about 10 Pa and voltage is raised high. The current at that time is about several 10 mA. This discharge is continued more than several hours.

Since D_2 gas comes out from the Pd rod and wire at the beginning of the discharge, the plasma covers the entire electrode as shown in Fig. 8. After that, when the gas is exhausted from the wire and rod, the whole inside of the reactor emits blue plasma as shown in Fig. 9.

After this processing, the final step is taken. Keeping the pressure intact, electric power is supplied to the ceramic heater, and the ceramic heater temperature is raised to 700–800°C. Figure 10 shows a photograph at the time of

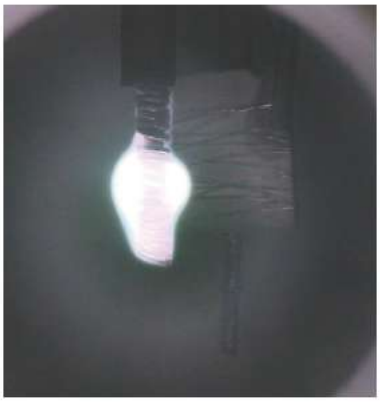

Figure 8. Photo of plasma.

heating by the ceramic heater. The heater shows red incandescence. This state is continued for about 10–20 h, and Pd is deposited on the nickel surface. Doing this produces the conditions needed to generate excess heat.

2.6. Air flow measurement for heat calibration

The same type of reactor is used in the calibration, and is installed as a control for calibration of the heat balance in the enclosure described below. The design, size, weight, and shape of this calibration reactor are exactly the same as the reactor used for testing. The internal reactants are the same nickel, of the same weight, size, dimensions and position. Both are washed and wound the same way. However, excess heat is not produced by the calibration electrode even though deuterium gas is added to the cell, because the nickel material is not processed as described in Section 2.5.

Figure 11 shows the test and calibration reactors. The latter reactor is placed in the calorimeter to obtain test and calibration data, and to demonstrate a heat balance of zero. Both reactors are shown in the photo. These can be tested

Figure 9. Photo of plasma.

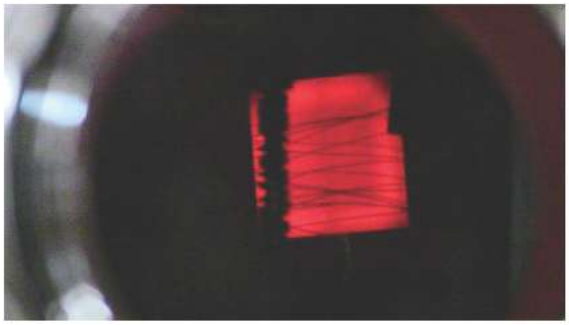

Figure 10. Photo of the ceramic heater.

separately, or at the same time. In this photograph, the calorimeter enclosure is removed. This enclosure will be described below.

The test or calibration reactor were placed in an enclosure, which is an acrylic box (Fig. 12) width 0.4 m, depth of 0.75 m, and height 0.7 m. Air-passage openings of 50-mm-diameter were made at the top and the bottom side of the box. A blower of 12 V, 0.6A, 7.2 W was installed on the top air-passage port. A platinum temperature sensor was positioned in the air outlet pipe of the blower set in the top hole of the box, and another sensor was positioned at the bottom air inlet hole. The blower is made by Sanyo Denki Instruments (San Ace B97, Model 109BM12GC2-1) and it is shown in Fig. 14. The periphery of the air outlet was covered with a paper cylinder having a length of 200 mm, and

Figure 11. Photo of the reactor.

Figure 12. Photo of the acrylic calorimeter enclosure.

the periphery thereof was further wrapped with aluminum foil insulation.

The blower was supplied with 5 W (constant voltage of 12 V, 0.42 A). The voltage and current data of the blower were continuously recorded by a PC. The air flow rate of the blower was calibrated with a digital anemometer (Custom Co. Ltd. CW-60) that shows Fig. 15. The thermoelectric anemometer ranged from 0.2 to 20 m/s, the resolution was 0.1 m/s, and the measurement temperature range was 0–50°C. The temperature of the air outlet and the wind speed were measured continuously by the equipment by the location of the outlet. In this way, the air leaving the blower was sufficiently agitated. An anemometer equipped with an air volume and a thermometer was used to confirm that both the wind speed and temperature were uniform. From the air volume and the air heat capacity, the temperature at the outlet from the box rises by about 0.05° per 1 W power input. Since the resolution of platinum temperature sensor is

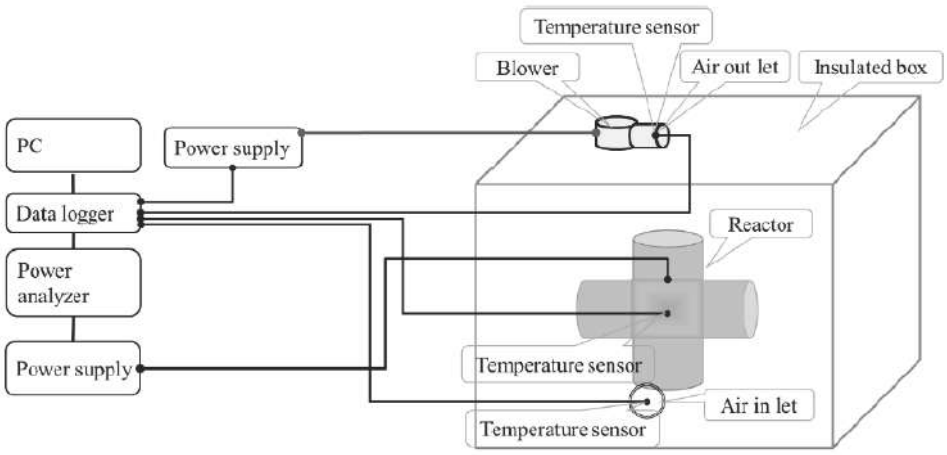

Figure 13. Schematic of measurement system.

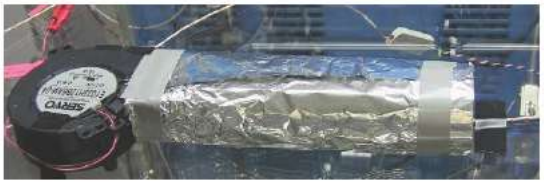

Figure 14. Photo of blower.

0.1°, power can be measured to the nearest ∼2 W.

Figure 13 shows a schematic of measurement system. The test reactor and calibration reactor are set in the center of the enclosure, and the control and the measuring system is shown on the left-hand side.

The rectangles in the lower left of the figure represent the input power supply, the power input analyzer (Yokogawa, PZ 4000), the data logger (Agilent, 34970A), and the PC for data acquisition. A capacitance diaphragm gauge (MKS Co. Ltd.) was used as the reactor's inner gas-pressure gauge. Data from six reactor temperatures, electric power to the test reactor that is processed by the power-meter, electric currents and voltages for the power supply of the blower, and the temperatures of the inlet and the outlet air flows were collected by a data logger and recorded to a PC every 5 s.

The reactor and the calibration reactor are set at the same position in the box. A constant volume of air was flowed from the bottom hole of the box. The air passes through, blowing on both the test reactor and the control reactor. It then goes out through the top hole of the box. The temperature of the inlet air was continuously measured with a platinum temperature sensor. A blower was installed at the upper air outlet port, and another temperature sensor was attached to the outlet hole. This sensor was installed at the air coming out of the blower.

The specific heat of constant pressure air of C_{p} is hardly affected by temperature. The C_{p} is described below. It is 1.005 J/g/deg at 273 K and 1.012 J/g/deg at 373 K and 1.026 J/g/deg at 473 K. The temperature of the air under test will be described later in the measurement example. In a typical measurement, the room temperature was 293 K and the maximum temperature of the air outlet was 333 K. In this case, the heat capacity of the warmed air increased by 0.3%. The temperature dependence of the heat capacity of air has a linear relationship with the temperature in the measurement range, and it can be expressed by Eq. (1). The first term and the coefficient of the second term of the equation are constants, and T_{out} is the temperature of the air outlet. These temperatures are continuously measured at both the air inlet and outlet. However, the influence of the factor is 1/10 or less of the measurement error that is

Figure 15. Air volume measurement tool for calibration.

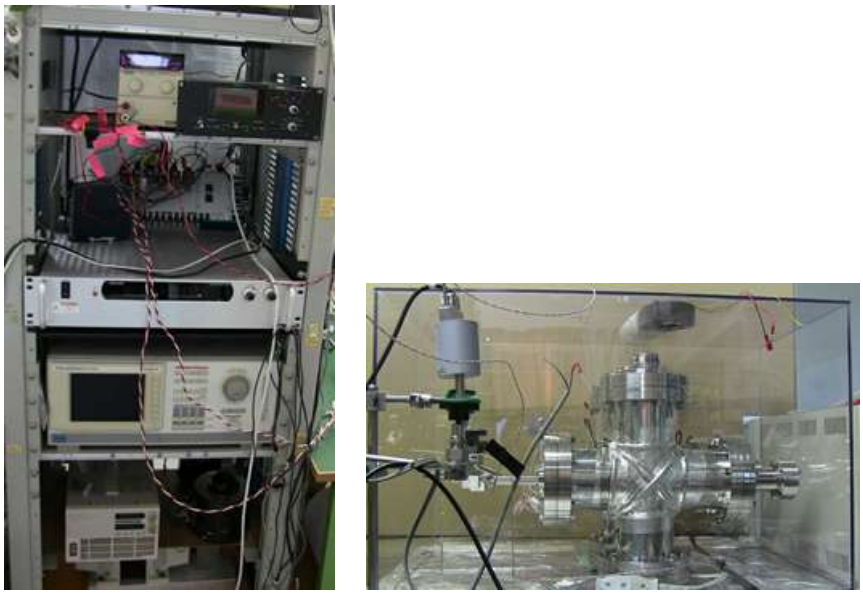

Figure 16. Photo of the measurement system and reactor in the shielding box.

described later.

$$H_c = 0.987 + 0.0000661 \times T_{out}. \quad (1)$$

The thermal calculations were carried out as follows. The input energy H_{in} was estimated as Eq. (2).

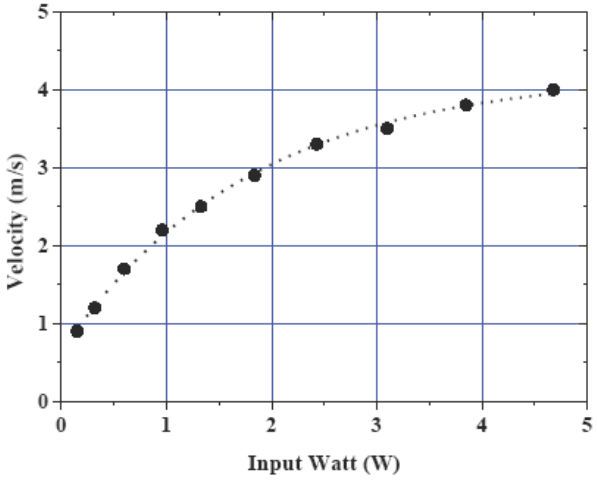

Figure 17. Relationship between the input power and the air velocity of the blower.

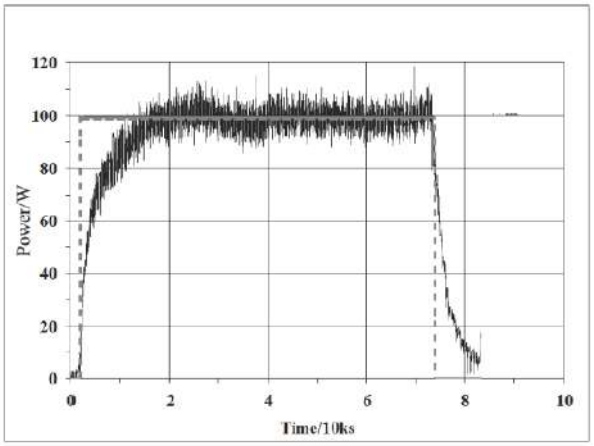

Figure 18. Changes of input and output power obtained reactor before excess heat generation treatment at 100 W of input power.

$$H_{\text{in}} = \sum_{0}^{T} \Delta W \times \Delta \text{t}, \tag{2}$$

where ΔW is the power at each time and Δt is the data integration time interval (24.47 s). Thermal output energy H_{out} was calculated as Eq. (3).

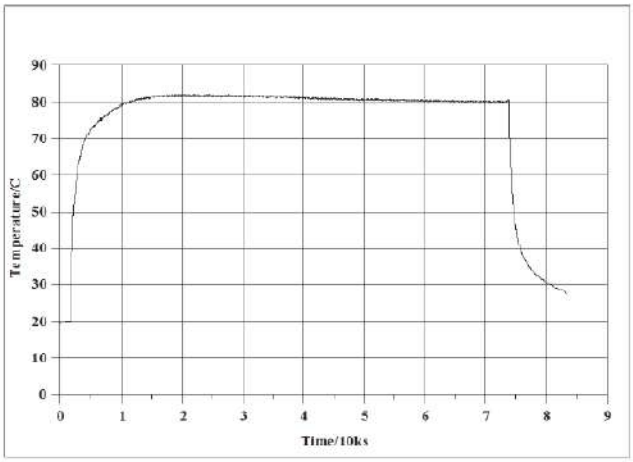

Figure 19. Temperature changes for outside body of reactor center at 100 W of input power before excess heat generation treatment.

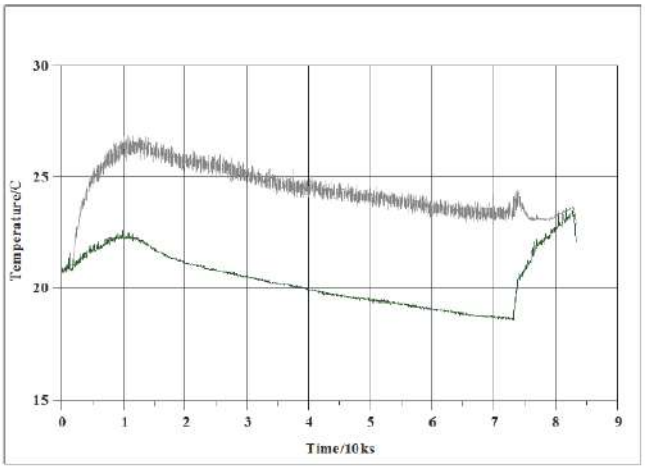

Figure 20. Temperature changes for inlet and outlet of the air at 100 W of input power before excess heat generation treatment.

$$H_{\text{out}} = \sum_{0}^{T} \Delta V \, S \, \rho \, Hc \, \Delta t \, dT, \tag{3}$$

where V is the wind velocity (m/s); S is the area of the air outlet, 8.2×10^{-3} m^2; ρ is the air density, 1.293 kg/m^3 at 273.2 K. This value is numerically presented as Eq. (4).

$$\rho = 3.391 \exp(-T_{\text{out}}/201.26) + 0.41529. \tag{4}$$

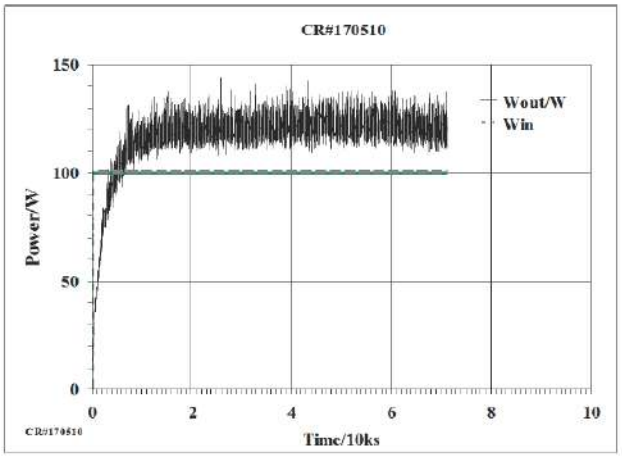

Figure 21. Test results obtained reactor during activation at 100 W of input power.

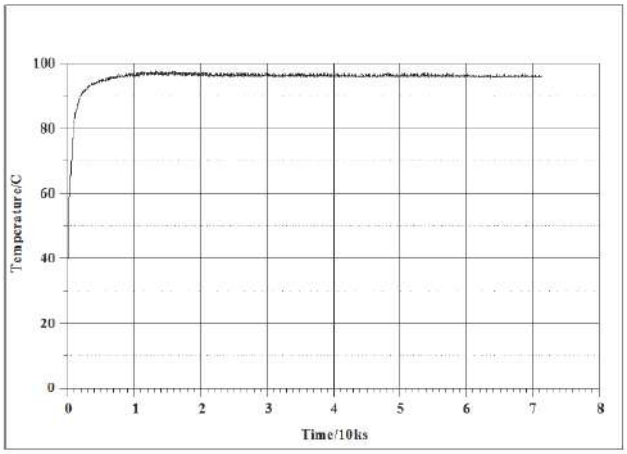

Figure 22. Temperature changes for outside body of reactor center at 100 W of input power during excess heat generation treatment.

The wind velocity at the flow meter was estimated by semi empirical Eq. (5).

$$V = A\exp(-W_{\mathrm{b}}/w) + B, \tag{5}$$

where A is a constant, -3.7; $B = 4$; $w = 1.375$; W_{b} is the blower input (W); and dT is the temperature difference between the air inlet and the outlet, $T_{\mathrm{out}} - T_{\mathrm{in}}$. In calculating the caloric value of air, the caloric value varies depending on atmospheric pressure and humidity in addition to temperature. The atmospheric pressure was calibrated with a commercially available barometer made by Sunoh company and humidity by a measuring instrument made by Empex company. There was no significant change during the 80 ks measurement period.

Figure 17 shows the relationship between the blower input and the air flow rate obtained from the air volume calibration results. In this figure, the black circle is the measured value, and the dotted line is the approximate expression value obtained measured values and expressed by Eq. (5). Data corresponding to the input power for the blower were also collected during the test. Blower input power was approximately 4–6 W. These results indicate that the heat can theoretically be calculated from the air flow rate, the difference between the temperatures of the air in and the air out, and the air heat capacity. However, we also calibrated the heat balance with the control reactor.

In a usual test, the input power of the blower is 5 W, so the wind speed is 4 m/s. Since the air outlet sectional area is 4.4×10^{-3} m^2, air volume of about 1.6×10^{-2}m^3/s passes through the interior of the box. Since the volume of the box is 0.21 m^3, if the air volume by the blower is 0.03 m^3, the air in the box is replaced every $\sim$13 s. We confirmed the flow of air using incense smoke. Air entering from the lower air inlet and directly hits the reactor body and then turns to the other side of the reactor. After that, the air rises to the top of the box and exits from the air outlet. We confirmed that the air passes through the entire interior of the box in a few seconds.

3. Results

3.1. Excess heat

The calibration test by control reactor results are shown in Fig. 18. Input power of 100 W was supplied for 2 ks to the control reactor. Output power increased until 20 ks, and then became constant. Input power was stopped at 73 ks and the heat output decreased to 0 W. The D_2 gas pressure in the reactor is 760 Pa. The amount of deuterium gas

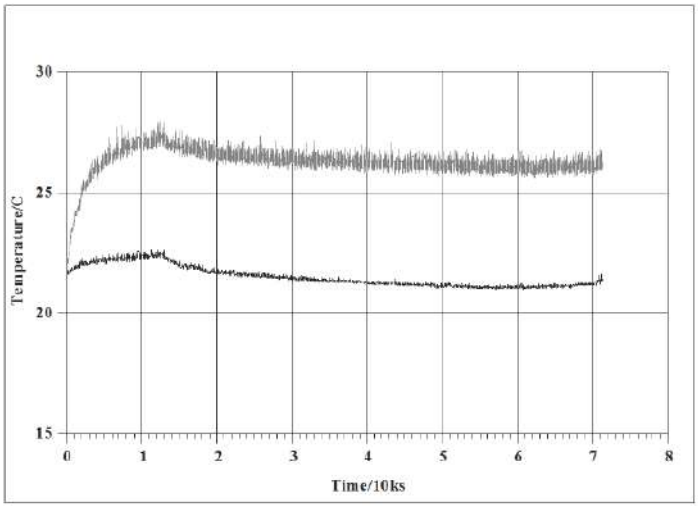

Figure 23. Temperature changes for inlet and outlet of the air at 100 W of input power before excess heat generation treatment.

is calculated as 20 cm^3 at the standard state. After reaching 100 W output, since there is no excess heat, it is almost constant at 100 W. The input was 100 W $\times$ 71.46 ks $=$ 7.15 MJ, and the output was estimated as 7.05 MJ; thus, the output/input ratio was 0.986. We consider this a reasonable calibration of the control reactor, and we assume the heat unaccounted for was lost by radiation from the box.

Figure 19 shows the change in reactor temperature with input of 100 W to the reactor before excess heat is produced. The temperature is the central temperature outside the reactor body that is shown in Fig. 1. When the room temperature is 21°, at the input of 100 W it reaches 80° Celsius after 10 ks. However, the other parts of the reactor body are lower than this temperature. This temperature is the value of the highest reactor body part.

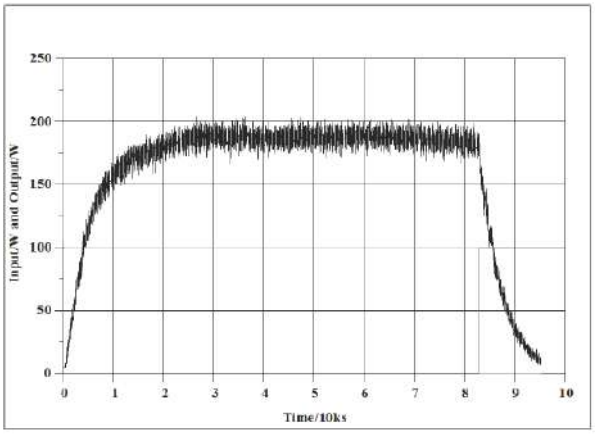

Figure 24. Changes for input and output power for the reactor after treatment of 100 W input.

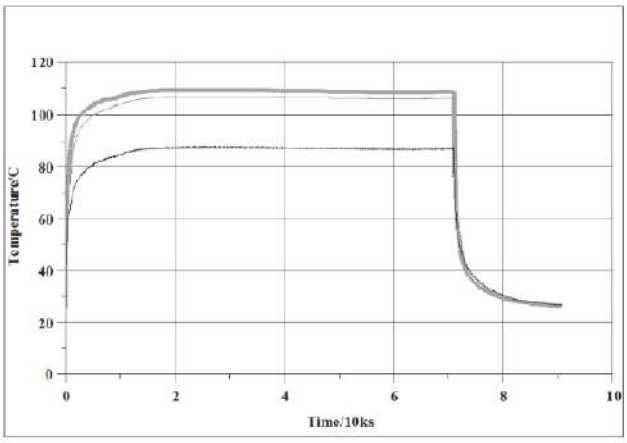

Figure 25. Temperature changes for various position of the outside body of reactor at 100 W of input power after excess heat generation treatment.

Figure 20 shows the temperature changes at the air inlet and outlet during the 100 W calibration. The temperature difference between outlet and inlet reaches 4.5°C at 10 ks after input power is supplied. The inlet temperature is almost the same as the room temperature, which changes by about 5° over the course of one day (i.e. 86 400 s), because there is no air conditioner in the laboratory. The air temperature changes, but the outlet minus inlet temperature difference is nearly constant.

Figure 21 shows the change in power in and power out when 100 W is input to the reactor during the treatment to produce excess heat. The D_2 gas pressure in the reactor was 760 Pa, the same as before (Figs. 18 and 21). Compared to Fig. 18, the output reaches 100 W at 5 ks. This is because excess heat was already being generated, with output of almost 120 W. The input stopped at 70 ks. Thereafter, additional evacuation and discharge processing are performed to increase the amount of excess heat generation.

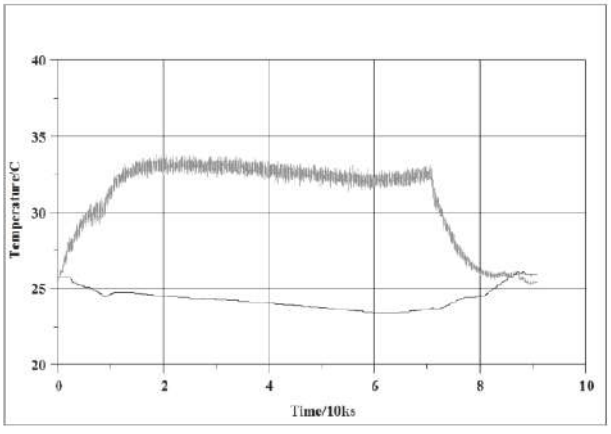

Figure 26. Temperature changes for inlet and outlet of the air at 100 W of input power after excess heat generation treatment.

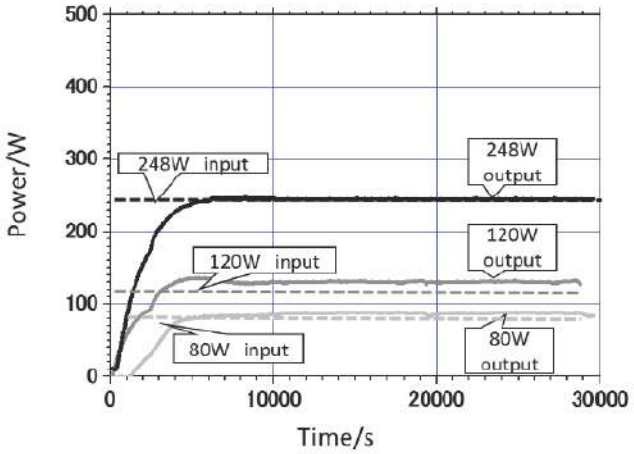

Figure 27. Change in output for calibration reactor.

Figure 22 shows the temperature change of reactor body over time. The temperature is 15°C higher than before the treatment (as shown in Fig. 19).

Figure 23 shows the temperature changes at the air inlet and outlet. The temperature difference between the outlet and inlet reaches 5°C at 10 ks after input power is supplied. The inlet temperature (i.e., room temperature), changes by few degrees during one day, but the outlet minus inlet temperature difference remains constant. The variation of the air inlet temperature is 0.2°C, and the variation of the outlet temperature is about 0.5°C. This is presumably because the amount of excess heat generation varies.

Figure 24 shows the change in power output when input of 100 W to the reactor during after the treatment for excess heat generation. The D_2 gas pressure in the reactor was 760 Pa, the same as before (Figs. 18 and 21). Compared with

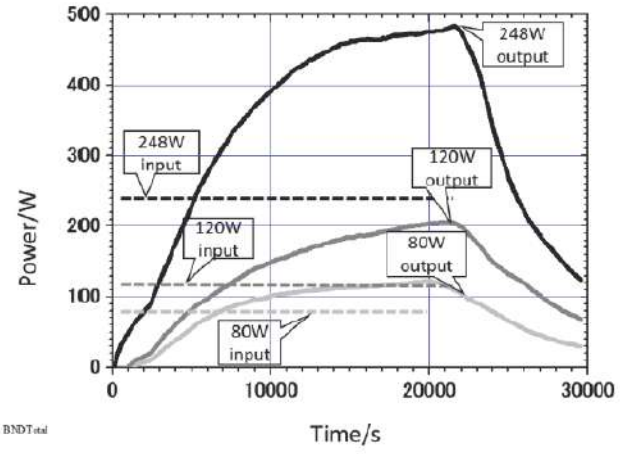

Figure 28. Change in output when input is changed to test reactor.

Fig. 18, the output reaches 100 W at 10 ks. The excess heat was continuously generated, which shows the output power has increased to 180 W. The input power was stopped at 82 ks. The input heat was 100 W $\times$ 82.5 ks $=$ 8.25 MJ, and the output heat was estimated as 15.19 MJ; thus, the output/input ratio was 1.841.

Figure 25 shows three position of temperature changes for outside body of reactor center and reverse side of the center, and 100 mm from the center of the reactor at 100 W of input power during excess heat generation treatment.

The temperature of the reactor body varies depending on the position. Nickel as a reactant is not present on the entire inner surface of the reactor. As can be seen from Fig. 1, the heater covers only the center portion of the reactor body. Therefore, the temperature varies from place to place in the reactor. The temperature is stable.

Figure 26 shows the temperature changes at the air inlet and outlet. The temperature difference between the outlet and inlet reaches 9°C at 20 ks after input began. The inlet temperature changes by 3°C over the course of 1 day, but the temperature difference between the outlet and inlet is constant. The changing of the air inlet temperature is 0.1°C, and the changing of the outlet temperature is about 0.5°C. This presumes that the amount of excess heat generation is stable.

The calibration test by the control reactor were performed at three input power levels. Figure 27 shows the output power of the control reactor for the input of 80 W, 120 W and 248 W. The output power is confirmed to be the same as input power.

The results of same inputs to the test reactor are shown in Fig. 28. These tests behave differently from the calibration test. The output increases with time. For example, 248 W input is made for 22 ks, the power output reaches 480 W and the Out/In ratio reaches 1.953. The generated power reaches two times input power.

The results of the calibration reactor and the heat generation test by vacuum reactor is shown in Fig. 29. The horizontal axis represents the input power, and the vertical axis represents the value obtained by subtracting the input power from the measured value, that is, the excess power (W_{ex}). The black rectangle mark is the result of the control reactor. As the input increases, the amount of radiation loss due to the temperature rise increases, and the output power becomes lower than the input. As a result, this excess is negative. When there is no deuterium gas (vacuum: indicated by triangle mark) in the reactor indicated by the same results line, the power balance is zero. Given the expected

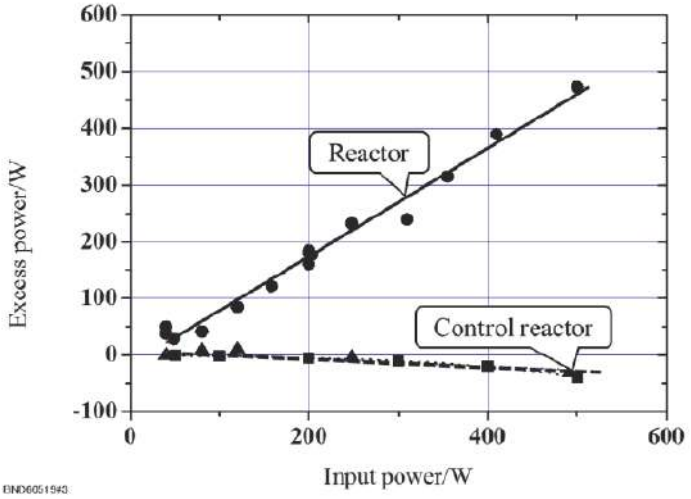

Figure 29. Comparison of several test for various interior reactor conditions.

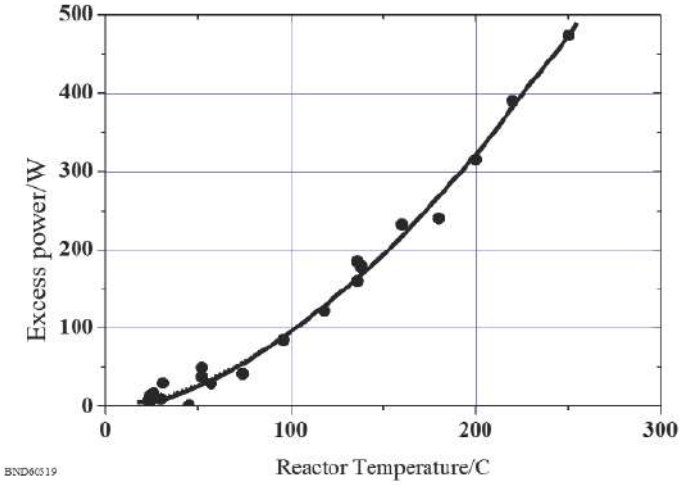

Figure 30. Relationship between excess power and reactor temperature.

losses, a balance of zero indicates slight excess power. This slight excess power is presumed to have been generated by deuterium gas remaining in the reactor. In the excess power generation test indicated by the black circle mark, the reactor body temperature rises as input increases, and as a result, the excess power increases. In this test, excess power is 160 W at 200 W of input power and it increases to 480 W at 500 W of input power.

The relationship between excess power (W_{ex}) and reactor temperature is shown in Fig. 30. The excess power increases with the temperature rise of the reactor. For example, the excess power is 100 W at 100°C, 315 W at 200°C, and 480 W at 250°C. Excess power of 10 W and 20 W was generated even when the reactor was near room temperature.

3.2. Observation of reacting metal

SEM observation of nickel surfaces before and after treatment are shown in Figs. 31 and 32. The surface roughness after processing is remarkable, and its size is not uniform. The particle size was distributed in the range of several tens to 0.001 mμ.

The distribution of Pd on the nickel surface after treatment is shown in Fig. 33. In this photograph, it is indicated

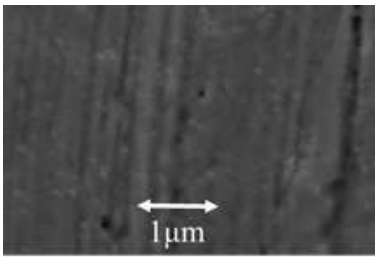

Figure 31. SEM photo of Ni reactant before treatment.

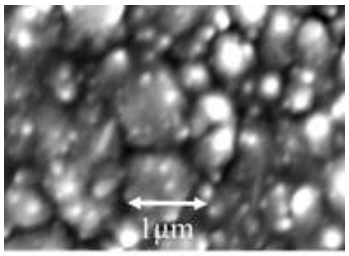

Figure 32. SEM photo of Ni reactant after treatment.

by purple dots. It is almost uniformly distributed. With unprocessed nickel, it is impossible to generate excess heat at all. However, if the surface is covered with particles and further Pd is present on the surface, excess heat is easily generated. The smaller the particles are, and the more Pd is uniformly present, the more the excess heat is generated.

Figure 34 shows the distribution of oxygen after treatment of Ni reacting metal. There is no oxygen observed. When such oxide film, nitride film or carbon are present in large amounts, it is difficult to generate excess heat. Removing impurities completely from reactant metal is one of the important conditions for successful excess heat generation.

Figure 35 shows a SEM image of the nickel mesh after generating 10^9 J of excess heat. Many cracks and peeled parts on the metal surface are observed.

Figure 36 is an enlarged photograph of the sample in Fig. 35. Many granular precipitates are observed on the surface.

Figures 37–39 show the distribution of oxygen, carbon, and nitrogen, respectively. These elements are widely present on the nickel wire surface. In particular, it can be seen that a large amount of carbon is present. It is possible these elements were originally present inside the reactor. However, it is clear that these elements increase on the electrode surface as the excess heat increases.

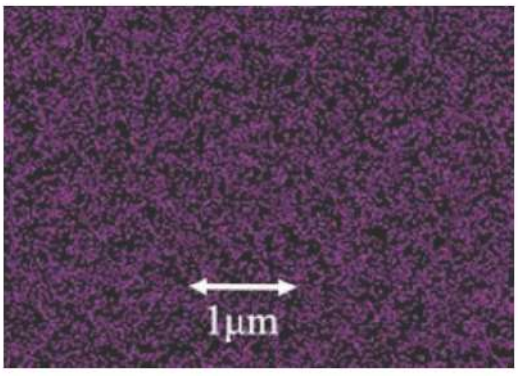

Figure 33. SEM photo of Pd distribution after excess heat generation.

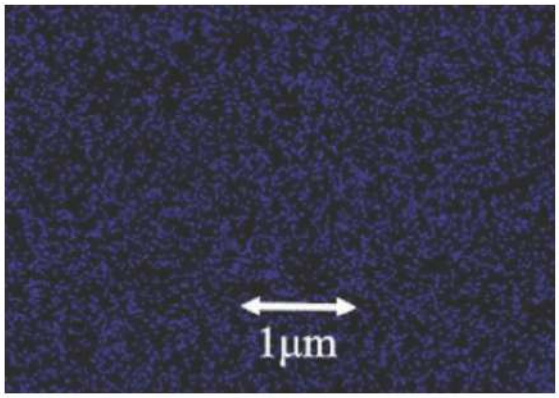

Figure 34. SEM photo of Oxygen distribution after excess heat generation.

4. Discussion

When the temperature of the reactor (T_{r}) is expressed as the reciprocal of the absolute temperature, as shown in Fig. 40, the excess heat relationship is linear. We speculate that the excess heat would reach the order of kilowatts at $1/T_{\mathrm{r}} = 0.001$, i.e. at T_{r} of approximately 700°C. We confirmed that the excess heat increases exponentially with reactor temperature. The reaction activation energy E_{a} was calculated on the basis of the linear region between 100 and 523°C in Fig. 40 to be 0.165 eV/K/atom.

A test with this reactor lasts almost 30 days. Typical excess heat during the time is estimated as 300 W. Total energy is thus $\sim 2.6 \times 10^8$ J. The amount of D_2 used was 20 cm^3 STP. Assuming that the reaction is D+D fusion, and assuming that all gases react, the amount of gas required to generate this much energy is approximately 12 cm^3 STP. Although this is a very rough calculation, this value coincides with the amount of gas consumed. Granted, this calculation is totally speculation, and there more data is needed to confirm it and to infer the reason for it.

To confirm the anomalous heat generation of the deuterium–metal system, complex thermal factors were narrowed

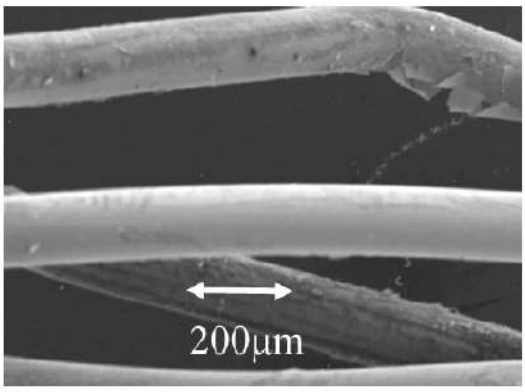

Figure 35. SEM photo of Ni wire after excess heat generation.

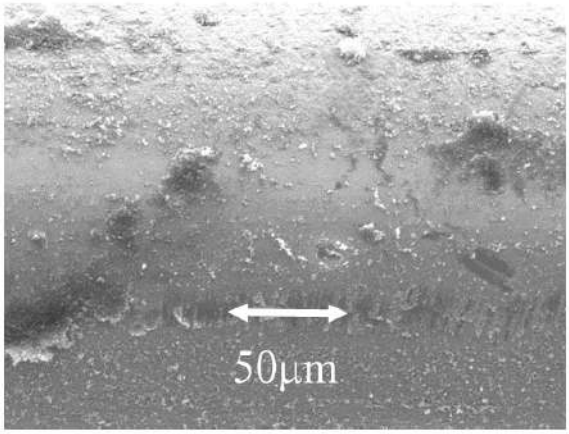

Figure 36. SEM photo enlarged photo 35.

down to two simple factors and analyzed. As a result, we confirmed the occurrence of the anomalous reaction. Factors for thermal analysis are required to change the amount of heat depending on the input power, the amount of flowing air, and the air inlet and outlet temperatures. On the basis of this thermal analysis and the results presented in this work, we presume that the method necessary for anomalous heat generation is as follows:

(1) Activation of the sample surface to make a fine structure, and addition of surface modification metal.
(2) Cover the surface with activated deuteride.
(3) Removal of impurities in the gas.
(4) Control of the reactor temperature and the deuterium gas pressure.

Activation of the metal surface, that is, removal of the oxide, nitride, and carbide layers, is particularly important. Heating and discharge treatment in deuterium gas is an effective method of activating the metal surface. The use of

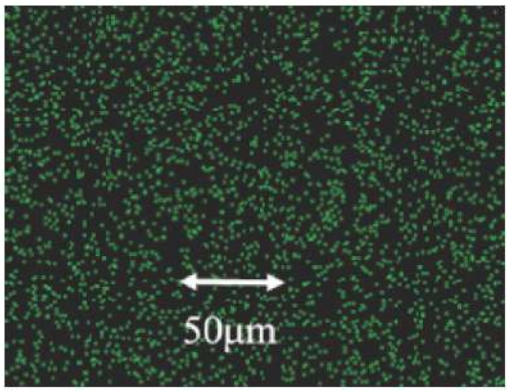

Figure 37. SEM photo of oxygen distribution.

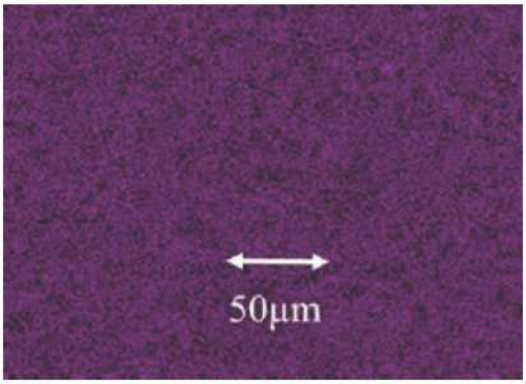

Figure 38. SEM photo of carbon distribution.

highly pure gas and the thorough removal of released gas during the surface treatment are also important. After a reaction metal sample has been fabricated, the activation treatment, where the sample is maintained under a hydrogen gas atmosphere at high temperatures, dissociates deuterium molecules into atomic deuterium on the metal surface, and the amount of dissociated deuterium increases with increasing treatment time. The presence of this atomic deuterium is presumed to be a necessary condition for excess heat. The occurrence of excess heat depends on the temperature, and it is at least on the order of a hundred watts. The excess heat calculated on the basis of the assumption that the reactant was nickel was several 10 W/g and was 1–10 W/cm^2.

Appendix A

In 2017, we developed a new, simplified method of preparing the electrode material that produces higher heat with better reproducibility. It includes the following steps.

Using 180 mesh nickel.

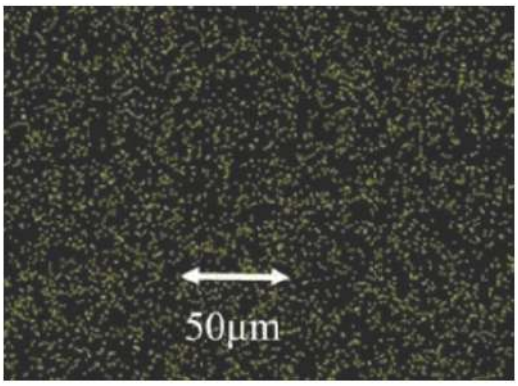

Figure 39. SEM photo of nitrogen distribution.

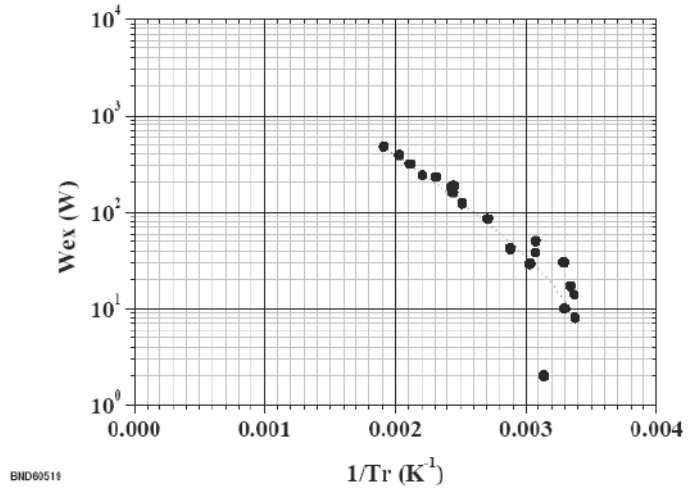

Figure 40. Relationship between excess heat and the inverse of the absolute temperature T_r of the reactor.

(1) Polish the mesh surface with grade 500 emery paper, and then with grade 1000 paper.
(2) Wash the surface with hot water. Detergents and the like should be avoided because they may contaminate the surface.
(3) Rub the surface with pure palladium. The palladium will adhere to the mesh. Alternatively, the palladium can be plated onto the mesh (plating solution: Tanaka Inc., PDMO2LB). This is the key step. In an industrial process, a similar material might be fabricated by some other method such as Nano-sintering.
(4) Place the mesh in the reactor. Evacuate to degas the mesh.
(5) Leaving the sample in the vacuum, additional degassing is performed by raising the temperature in stages to 100, 200 and 300°C.
(6) Introduce D_2 or H_2 gas at 100–700 Pa, and lower the temperature to room temperature to absorb the gas.

We have tested a Pd on a pure Ni surface. We are currently testing with this method. We will describe these results in more detail after enough results have been obtained. In this paper we described only about heat generation. We also analyze neutrons, gamma rays, transmutation, gas analysis and gas isotope analysis. We mainly analyze the correlation between these results and heat. We are preparing to publish a paper on these results.

We believe other metals might be substituted for Pd on Ni, and they might perform better. Pt might be a good candidate.

Acknowledgments

Special thanks are extended to David Nagel for kindly reviewing our manuscript. We also thank Steve Krivit, Dewey Weaver, Hideki Yoshino and Jed Rothwell for support of this study. The author is also grateful for support from the late John O'M Bockris and the late Richard Oriani.

References

[1] M. Fleischmann, S. Pons and M. Hawkins, *J. Electroanal. Chem.* **261** (1989) 301.

[2] S. Pons and M. Fleischmann, *J. Electroanal. Chem.* **287** (1990) 293.
[3] M. Fleischmann and S. Pons, *J. Electroanal. Chem*. **332** (1992) 33.
[4] M. Fleischmann and S. Pons, *Phys. Lett. A* **176** (1993) 118.
[5] M. Fleischmann M and S. Pons, *Phys. Lett. A* **187** (1994) 276.
[6] J.E. Jones, E.P. Palmer, J.B. Czirr, D.L. Decker, G.L. Jensen, J.M. Thorne, S.F. Taylor and L. Rafelski, *Nature* **338** (1989) 737.
[7] T. Mizuno, T. Akimoto, K. Azumi, M. Kitaichi and K. Kurokawa, *Fusion Technol.* **29** (1996) 385.
[8] T. Mizuno, T. Ohmori, T. Akimoto and A. Takahashi, Jpn. *J. Appl. Phys*. **39** (2001) 6055.
[9] T. Mizuno, T. Akimoto, T. Ohmori, A. Takahashi, H. Yamada and H. Numata, *Jpn. J. Appl. Phys.* **40** (2001) L989.
[10] T. Mizuno, T. Ohmori, K. Kurokawa, T. Akimoto, M. Kitaichi, K. Inoda, K, Azumi, S. Shimokawa and M. Enyo, *Denki Kagaku Oyobi Kogyo Butsuri Kagaku* **64** (1996) 1160 (in Japanese).
[11] S. Forcardi, R, Habel and F. Piantelli, *Il Nuovo Cimento* **107A** (1) (1994) 163–167.
[12] S. Forcardi, R, Habel and F. Piantelli, *Il Nuovo Cimento* **111A** (11) (1998) 1233–1242.
[13] E. Cerron-Zeballos, I. Crotty, D. Hatzifotiadou, J. Lamas Valverde, M.C.S Williams and A. Zichichi, *Nuovo Cimento* **109A** (1996) 1645–1655.